



# Seasonal variability in aeolian dust deposition fluxes and their mineralogical composition over the Northeastern Arabian Sea

K. Suresh<sup>1,2</sup> · A. Kumar<sup>1</sup> · V. Ramaswamy<sup>1</sup> · C. Prakash Babu<sup>1</sup>

Received: 21 October 2020 / Revised: 6 June 2021 / Accepted: 23 June 2021 / Published online: 7 July 2021  
© Islamic Azad University (IAU) 2021

## Abstract

Atmospheric mineral dust is derived from arid/semi-arid region, undergoes long-range transport, and can impact surface biogeochemical processes in the pristine marine region. This study reports fluxes of mineral dust (wet and dry deposition), their clay mineralogy, and associated seasonal variability over the Northeastern Arabian Sea. Dust sources are assessed using mineral composition and their ratios as well as satellite retrievals during 2012–2015. The average wet deposition flux ( $293 \text{ mg m}^{-2} \text{ day}^{-1}$ ) of mineral dust is three times higher than dry deposition flux ( $96 \text{ mg m}^{-2} \text{ day}^{-1}$ ). A clear distinction is observed in the mineral composition of wet and dry deposited dust with smectite and palygorskite being dominant during the wet period and illite and chlorite being dominant during the dry period. Mineralogical composition and their ratios indicate that major dust sources to the Northeastern Arabian Sea are from northeast Africa, Arabian Peninsula, and southwest Asia. These observations are corroborated with the satellite retrievals, aerosol optical depth, and back trajectory analyses.

**Keywords** Aeolian dust · Arabian Sea · Deposition flux · Clay minerals · Long-range transport

## Introduction

Mineral dust has many effects on the Earth's radiation budget, ecosystems, and ocean productivity (Claquin et al. 2003, 1999; Tegen et al. 1996; Jickells et al. 2005; Guieu et al. 2019). It plays a significant role in providing nutrients to marine and terrestrial ecosystems (Mahowald et al. 2018, 2005; Jickells et al. 2016, 2005; Jickells and Moore 2015; Banerjee and Prasanna Kumar 2014; Okin et al. 2004; Swap et al. 1992). The Arabian Sea, surrounded by major deserts and semi-arid regions, receives 113–154 Mt of dust every year (Duce et al. 1991; Ginoux et al. 2001). The Arabian Peninsula region is third-largest dust source in the world after the Saharan and East Asian dust sources (Kok et al. 2021; Goudie and Middleton 2006). Recent studies over the Arabian Sea have highlighted significant dust transport

toward the North Eastern Arabian Sea (NEAS) during the Southwest monsoon (June to September; Suresh et al. 2021), which have potential to impact rainwater chemical composition (Ramaswamy et al. 2017) as well as intensity and outbreak of monsoon (Vinoj et al. 2014). Apart from continuous dust transport during the southwest (SW) monsoon, many episodic dust storms are reported over the Arabian Sea during the dry season (October to May; Kumar et al. 2020). Sometimes, these dust storms are caused by the passage of extratropical cyclones (also known as western disturbances) originating from the Middle-east and SW Asia and transported toward the NEAS under favorable meteorological conditions (Badarinath et al. 2010, 2009; Ramaswamy 2014; Aswini et al. 2020). Subsequent to a storm event, dust particles undergo long-range transport to pristine marine and continental ecosystem. These dust particles also act as carrier for several limiting and co-limiting nutrients and toxicants (Jickells and Moore 2015; Paytan et al. 2009; Moore et al. 2013). These nutrients get deposited to surface water of ocean and can significantly modulate biogeochemical processes including primary productivity, which in turn can impact global carbon cycle (Coale et al. 1996; Watson et al. 2000).

Several studies, based on remote sensing data, have shown aeolian dust contribution from the Middle-East region,

Editorial responsibility: Mohamed F. Yassin.

✉ A. Kumar  
ashwinik@nio.org

<sup>1</sup> Geological Oceanography Division, CSIR-National Institute of Oceanography, Dona Paula, Goa 403004, India

<sup>2</sup> School of Earth, Ocean, and Atmospheric Sciences, Goa University, Goa, India



northeastern Africa (NEA), and southwest Asia (SWA) to the Arabian Sea (Ginoux et al. 2001; Goudie and Middleton 2006; Léon and Legrand 2003; Prospero et al. 2002; Aswini et al. 2020; Rashki et al. 2018; Rashki and Goudie 2021). In addition, several workers have made modeling effort to estimate dust fluxes and highlighted the impact of dust deposition on ocean productivity (Banerjee and Prasanna Kumar 2014; Guieu et al. 2019). However, very few attempts have been made to quantify dust fluxes based on ambient aerosol concentration (Tindale and Pease 1999), which will provide a more accurate value as compared to those obtained from remote sensing or numerical modeling methods. Moreover, very few attempts have been made so far, to characterize the clay mineral composition of aeolian dust over the Arabian Sea (Kumar et al. 2020). Clay mineral composition and their ratios can be used as a proxy for source identification and dust transport pathways (Caquineau et al. 2002; Rojas et al. 2019; Yu et al. 2019; Kumar et al. 2020). However, in the context of the Arabian Sea, a significant gap is found in the knowledge of the dust fluxes and their mineralogical composition.

In this study, wet deposition samples were collected during the SW monsoon of 2013, and aerosol samples collected during twelve major dust events of 2012–2015 in Goa (15.45° N, 73.80° E) over the Northeastern Arabian Sea were used to estimate the dust fluxes during the wet and dry period. In addition, dust clay mineralogical compositions have also been analyzed and used to assess their seasonal variability in conjunction with source composition. In combination with clay mineralogy, the results in this study are further supported by satellite-derived images and products, aerosol optical depth (AOD), 7-days back trajectory analyses, and CALIPSO profiles.

## Study area

The Arabian Sea is surrounded by arid and semiarid regions of the Arabian Peninsula and northeastern Africa on the west, Makran coast and endorheic basins of Iran, Afghanistan, and Pakistan, and the Thar Desert on the north, and humid tropical Peninsular India on the east. This basin experiences a seasonal reversal of winds; from June to September, the winds are southwesterly and from November to March are northeasterly (Fig. 1a, b). The SW monsoon period is also the primary rainy season and accounts for more than 80% of India's annual rainfall. Other major wind systems active in this region are Summer Shamal winds (from mid-May to mid-August) which flow from the Mediterranean Sea through the Middle-East to the Arabian Sea (Pease et al. 1998; Yu et al. 2016) and the Levar winds (mid-May to mid-September) which flow from central Asia to the northern Arabian Sea through the mountain gap between

the Palanghan and the Hindu Kush mountains (Alizadeh-Choobari et al. 2014; Rashki et al. 2019). From November to March, western disturbances, mainly originating in the Mediterranean Sea, propagate toward the Himalayas and last for short periods (1–5 days) (Madhura et al. 2014; Thoppil and Hogan 2010). These wind systems are strong enough to raise dust from the source regions and transport it to large distances. Apart from the above wind systems, several tropical cyclones form, before and after the SW monsoon in the Arabian Sea and Bay of Bengal, which have the potential to transport dust over the Arabian Sea depending on their location (Badarinath et al. 2009; Ramaswamy 2014).

Based on the available literature, major clay minerals present in the dust source regions have been compiled and are shown in Fig. 1c (Debrabant et al. 1991; Sirocko and Lange 1991; Alizai et al. 2012; Purnachandra Rao et al. 2015; Avinash et al. 2016; Yu et al. 2019; Kumar et al. 2020; Suresh et al. 2021). Northeast Africa is characterized by abundant smectite due to weathering of flood basalts and volcanic ejecta in the African Rift Valley; however, Somali Plains contain a significant amount of palygorskite (Alaily 1995; Singer et al. 1998). The Arabian Peninsula is characterized by high illite and palygorskite (Suresh et al. 2021 and references therein). The SW Asia, Indus Plains, and the Thar Desert are rich in illite and chlorite, due to sediments derived from mechanical weathering of rocks and sedimentary formations in snow-clad mountains (Vögeli et al. 2017; Alizai et al. 2012). The Indian Peninsula has high smectite and chlorite due to the weathering of Deccan Trap basalts (Purnachandra Rao et al. 2015). The characteristic composition of the major clay minerals in different source regions can be compared with those observed in the collected dust samples at the study site to assess the contribution from various sources.

## Materials and methods

### Sampling and X-ray diffraction analysis

Rainwater was collected using plastic trays during the SW monsoon period of 2013 (June to September) (Table 1) to obtain the dust settled through the wet deposition (Suresh et al. 2021). The trays were washed thoroughly before and after each sampling. The collected rainwater was filtered using polycarbonate filters (0.4 µm) to obtain wet deposited dust samples (WDS). The filtered WDS was dried, and the mass difference in the filter before and after filtration was obtained by weighing. The wet deposition flux is calculated by measuring the weight of the wet deposition sample obtained for 1m<sup>2</sup> area for one sampling day of the precipitation (Ramaswamy et al. 2017). Sixteen wet deposition samples, one sample per week, were chosen as representative



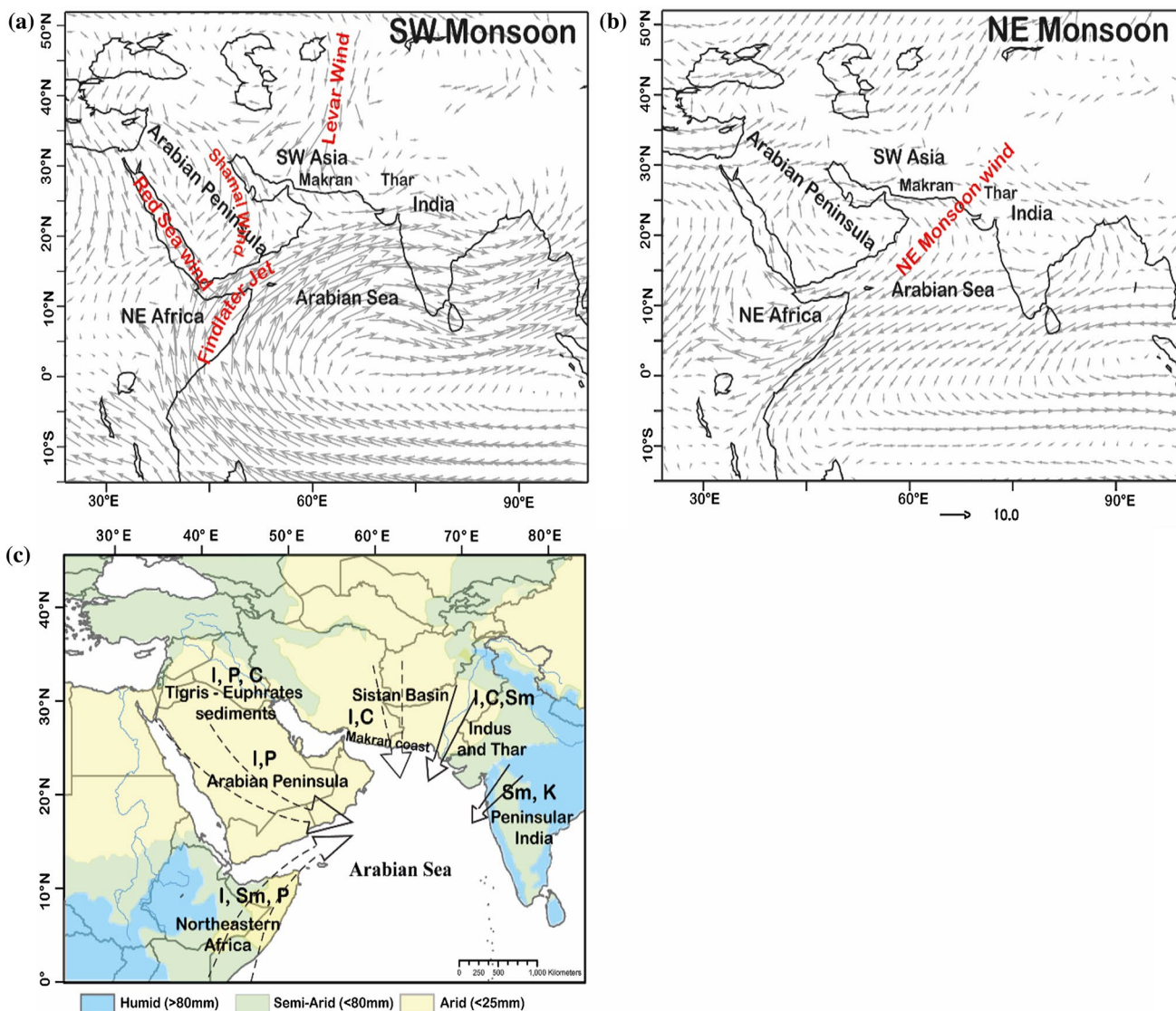


**Fig. 1** Map showing climatological wind data of the seasonal reversal of monsoon winds. **a** SW monsoon wind and Summer Shamal wind are consistent over the Arabian Sea and Arabian Peninsula respectively (June to September). **b** NE monsoon wind from the Indian subcontinent are prevalent over the Arabian Sea (January and February).

**c** Major clay minerals (I—illite, P—palygorskite, Ch—chlorite, Sm—smectite, and K—kaolinite) present in the source regions. Also shown the mode of Aeolian (dashed line) and fluvial (solid line) transport of mineral dust and sediments to the Arabian Sea (Debrabant et al. 1991; Sirocko and Lange 1991; Purnachandra Rao et al. 2015)

for clay mineralogical studies throughout the SW monsoon period. Slides for X-Ray diffraction of WDS were prepared by taking an aliquot of the samples collected, which were pretreated with 5 ml of H<sub>2</sub>O<sub>2</sub> to remove organic matter if any. The samples were made into a thick slurry and directly pipetted onto glass slides. After drying, the glass slides were glycolated for 12 h at 60 °C using ethylene glycol.

Bulk aerosol samples were collected during 2012–2015 (Table 2) in the campus of National Institute of Oceanography, Goa, India (15.45° N, 73.80° E), which is approximately 500 m away from the Arabian Sea coast (Aswini et al. 2020; Kumar et al. 2020). Whatman® GF/A glass fiber

filters (size 20 × 25 cm) were used as a substrate for aerosol sampling using a high-volume sampler with a flow rate of 1.0–1.3 m<sup>3</sup> min<sup>-1</sup>. The sampling period was typically varying between 22 and 24 h. The total suspended particulate (TSP) mass concentration was calculated by weighing the filters before and after sampling and normalizing with the volume of air pumped through the filter. The selection of aerosol samples during dusty days was considered with an anticipation of getting sufficient mass load on filter which can be subsequently used for mineralogical analyses. Major dust storms that reached the sampling site are detailed in Table 2, and aerosol samples collected during that period

**Table 1** Date of wet deposition collection, wet deposition dust flux, and the clay minerals relative percentages

Sample ID	Date of collection	Wet deposition flux (mg m <sup>-2</sup> day <sup>-1</sup> )	Smectite	Palygorskite	Illite	Kaolinite	Chlorite
WD-1	7-10th June 13	170	16	37	28	19	ND
WD-2	12th June 13	434	15	34	21	17	14
WD-3	18th June 13	449	27	33	14	16	10
WD-4	25th June 13	111	30	29	17	13	11
WD-5	30th June 13	166	33	19	23	11	13
WD-6	4th July 13	332	23	28	23	13	13
WD-7	13th July 13	379	38	21	16	13	12
WD-8	18th July 13	949	56	8	11	15	10
WD-9	25th July 13	569	43	18	17	12	10
WD-10	1st Aug 13	519	43	19	14	13	11
WD-11	7th Aug 13	124	20	22	25	18	15
WD-12	13th Aug 13	141	22	18	29	14	18
WD-13	20th Aug 13	76	30	20	15	13	22
WD-14	6th Sep 13	63	16	13	44	10	17
WD-15	20th Sep 13	127	ND	ND	50	22	28
WD-16	30th Sep 13	95	ND	ND	53	18	29

ND Not detected

**Table 2** Dry deposition sample name, the date of collection, dust flux, and the clay minerals relative percentages

Dust storm	Date of collection	Dry deposition flux (mg m <sup>-2</sup> day <sup>-1</sup> )	Smectite	Palygorskite	Illite	Kaolinite	Chlorite
DS-1	5–6 March 2012	132	23	ND	39	15	24
DS-2	24–25 March 2012	93	16	ND	35	12	37
DS-3	27–28 Dec 2012	115	15	ND	40	16	29
DS-4	6–7 Feb 2013	110	9	11	32	16	32
DS-5	10–11 April 2013	111	14	45	18	17	6
DS-6	9–10 May 2013	112	17	25	19	15	24
DS-7	12–15 June 2013	94	7	40	17	16	20
DS-8	10–11 April 2014	62	9	ND	49	15	27
DS-9	4–5 May 2014	62	11	ND	40	21	28
DS-10	14–15 Oct 2014	60	8	ND	62	8	22
DS-11	6–7 April 2015	116	11	38	20	20	11
DS-12	25–26 April 2015	80	20	ND	41	23	15

were analyzed for clay mineralogy. Oriented slides were prepared following the method developed by Kiefert et al. (1992). The filters were rinsed with Milli-Q water and ultra-sonicated for 30 min. Dust obtained in the tubes was subsequently sieved with a 230 ASTM sieve to remove any glass fibers present. In almost all filters, adequate dust was obtained for the XRD analysis from 1/8th of the filter. Filtered dust was treated with H<sub>2</sub>O<sub>2</sub> to remove organic matter present in the sample if any. The mineral dust was congregated by centrifuging, and excess water was removed from the tube. The dust extracted from the filters was used in the XRD analyses. The samples were pipetted onto glass slides

to make oriented slides and dried. The slides were glycolated for 12 h at 60 °C using ethylene glycol before XRD analysis.

The glycolated slides were analyzed under Rigaku® Ultima IV X-Ray Diffractometer with Cu K $\alpha$  radiation at 40 kV and 20 mA between 3° and 30° 2 $\theta$  at 0.02° 2 $\theta$ /s. Before the analysis of samples by X-Ray diffraction, the system was calibrated by using a silicon standard. Semi-quantitative determinations of relative mineral percentages were focused mainly on clay minerals present in the samples. Major minerals identified were illite, smectite, kaolinite, chlorite, and palygorskite. Peak area was calculated by taking the area of a particular mineral above an appropriate



baseline using the Rigaku Integral analysis 6.0 software. The relative mineral percentages were calculated by using the correction factors provided by Biscaye, (1965).

### Dust flux determination

To quantify dust concentration in aerosol samples, aluminum concentration is measured in the completely digested filters using strong acids. A one-eighth portion of the sampled filter was digested in Savillex vial (15 ml capacity) using a mixture of supra-pure HF and HNO<sub>3</sub> at 110 °C for 24 h under a clean laminar flow bench. The acid digestion process was repeated until the filters were completely dissolved. Post-dissolution, samples were dried and were transferred to pre-cleaned polypropylene bottles using 2% supra-pure HNO<sub>3</sub>. The Al concentrations were analyzed using ICP-OES (Agilent 710) following the methodology described in Kumar et al. (2020).

The dust fluxes were estimated based on the Al concentrations measured in collected samples. The abundance of Al was used as an indicator of the mineral dust in several studies to calculate the dust concentrations (Duce and Tindale 1991; Kumar and Sarin 2009; Anderson et al. 2016; Kumar et al. 2020), by presuming that the Al in mineral dust is same as in the UCC (upper-continental crust with Al content of 8.04%; McLennan 2001). We used an average settling velocity of 1000 m day<sup>-1</sup> for the estimation of dry deposition flux, following Shelley et al. (2015) and Anderson et al. (2016). For wet deposition, it was presumed that particulate collected after filtration is composed of mineral dust and wet deposition flux will provide an upper limit of dust deposition flux (Ramaswamy et al. (2017).

### AOD, satellite images, HYSPLIT backward trajectories, and CALIPSO profiles

Aerosol Optical Depth (AOD) and satellite images from the Moderate-resolution Imaging Spectroradiometer (MODIS) of Aqua and Terra satellites of NASA were used for tracking the dust storm regions. Time-averaged map of combined dark target and deep blue AOD at 0.55micron for land and ocean (<https://giovanni.gsfc.nasa.gov/giovanni/>) was used to monitor the dust activity and transport from the source region toward the Arabian Sea. Seven-day backward air mass trajectories have been computed to identify the possible dust source regions from where dust can be transported following the modeled trajectories. HYBRID Single-Particle Lagrangian Integrated Trajectory (HYSPLIT) model was used along with the GDAS meteorological dataset from the National Oceanic and Atmospheric Administration (NOAA) Air Research Laboratory (<http://www.arl.noaa.gov/ready/hysplit4.html>) (Rolph et al. 2017; Stein et al. 2015) to compute these back trajectories for sampling days. The model

was simulated for 168 h at different altitude ranges (mainly 500–1500 m, 1500–2500 m, and 2500–4000 m) above ground level during the wet deposition samples and dry deposition sampling days, to show the origin of dust-laden air mass at different altitudes from different source regions. Also, we investigated CALIPSO (Cloud-Aerosol Lidar Infrared Pathfinder Satellite Observations) profiles to identify the presence of dust in the region (available online <https://www-calipso.larc.nasa.gov/>) for the satellite passing over or near the sampling site for days before/after sampling days.

## Results and discussion

### Satellite images and AOD over the dust emission sources

Based on the AOD, satellite images, back trajectories, and CALIPSO profiles obtained over the Arabian Sea, sources of dust emissions were identified for the NEAS. Out of sixteen wet deposition samples collected, Fig. 2a, b is typical images showing high dust intensity (activity) at or near to the source regions (based on high area-averaged AODs) for two samples (WD-1 and WD-15) collected during the SW Monsoon period. 7-day back trajectories (for sampling days) are also superimposed on AOD maps to assess possible transport of dust from the source region to our sampling site (also refer to Fig. S1a to S1g in supplementary material S1 for rest of wet deposition sample collection days). These AOD maps highlight high dust activity over the western Arabian Sea (mainly the coastal Oman and Yemen), the Gulf of Aden, and the southern Red Sea (Fig. 2a). Between June and August, wind trajectories at 500–1500 m (Fig. 2a and Fig. S1a to S1g of supplementary material S1) follow the path of the SW monsoon winds. The major dust sources lying in the path of the SW monsoon winds are the Horn of Africa and coastal dust sources in the southern Arabian Peninsula. The SW monsoon wind also passes over the high AOD regions of the Gulf of Aden (Fig. 2a), which can receive dust from the Red Sea coastal deserts (Ramaswamy et al. 2017; Rojas et al. 2019). Trajectories at higher altitudes (>1500 m) follow the path of summer Shamal winds, which pass over dust sources located in Syria, Iraq, and the Arabian Peninsula. Ramaswamy et al. (2017) have shown that the dry and dusty summer Shamal and the Red sea winds override the moist SW monsoon winds and the dust is carried toward the west coast of India. The presence of dust is further substantiated from the CALIPSO close-pass images which give the vertical distribution of dust at or near to source/receptor region during the study period. The closest CALIPSO overpass observed near to sampling site (for WD-1 and WD-15) is given in Fig. 2c, d, respectively. The presence of dust aerosols is clearly visible from the aerosol distribution along the

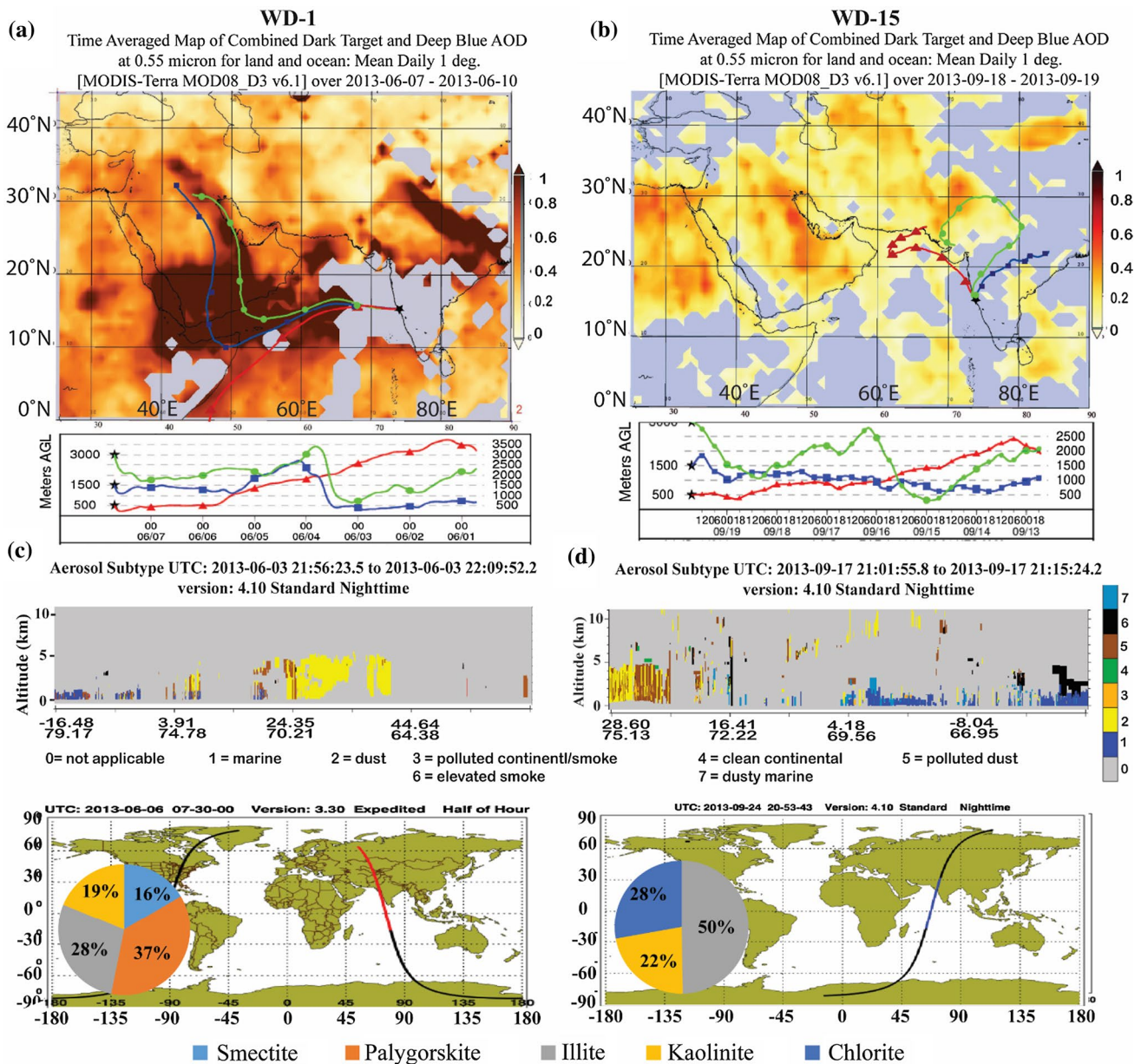


**Fig. 2** Map shows area-averaged AOD superimposed with 7-day air mass back trajectories ending at the Goa on sample collection date for wet deposition samples. **a** WD-1 and **b** WD-15 collected at the beginning and end of the monsoon, respectively. In **a** 500-m trajectory follows the Findlater jet path, whereas trajectories > 1500 follow the Summer Shamal path over the Arabian Peninsula. In **b**, the trajec-

track (Fig. 2c, d), as classified by CALIPSO vertical feature mask which uses an algorithm to classify seven aerosol types (Vaughan et al. 2004; Winker et al. 2009). Based on these CALIPSO profiles, it can be inferred that majority of dust transport occurs at relatively higher altitudes during SW Monsoon period, similar to those reported by Ramaswamy et al. (2017). As the ITCZ retreats south in September, the trajectories are mostly from the northern Arabian Sea,

which receives most of the dust from the arid landmasses in Iran, Afghanistan, and Pakistan (Goudie and Middleton 2006; Rashki et al. 2019) (Fig. 2b). We also observed relatively polluted dust (numbered as 5 in Fig. 2d) in WD-15 compared to that in WD-1, as the dominant source is SW Asia for DS-15, which has relatively higher anthropogenic emissions (Kumar et al. 2020).

tor is mainly from the northern Arabian Sea and over the SW Asian sources. CALIPSO passes near the sampling site for the sampling of **c** WD-1 and **d** WD-15, which shows the presence of dust (yellow is dust) over the Arabian Sea region. Also shown the pie chart highlighting relative fraction of clay minerals in dust collected

Among 12 dust samples collected during storm events reported in this study, eight were (DS-1, DS-2, DS-3, DS-4, DS-8, DS-9, DS-10, and DS-12) backtracked to dust sources in SW Asia like the Sistan basin, Makran coast, Jaz Moorrian basin, and Indus Delta. However, preliminary sources for four (DS-5, DS-6, DS-7, and DS-11) samples collected at the study site were found to derive from the Arabian

Peninsula. The preliminary source identification was carried out using the area-averaged map and 7-day back trajectory analyses, as discussed for wet deposited samples. Two dust collection days (for DS-2 and DS-5) AOD maps and back trajectories are shown in Fig. 3a, b, respectively. Similar AOD maps with back trajectories for other dust collection days are detailed in Supplementary material (Fig.

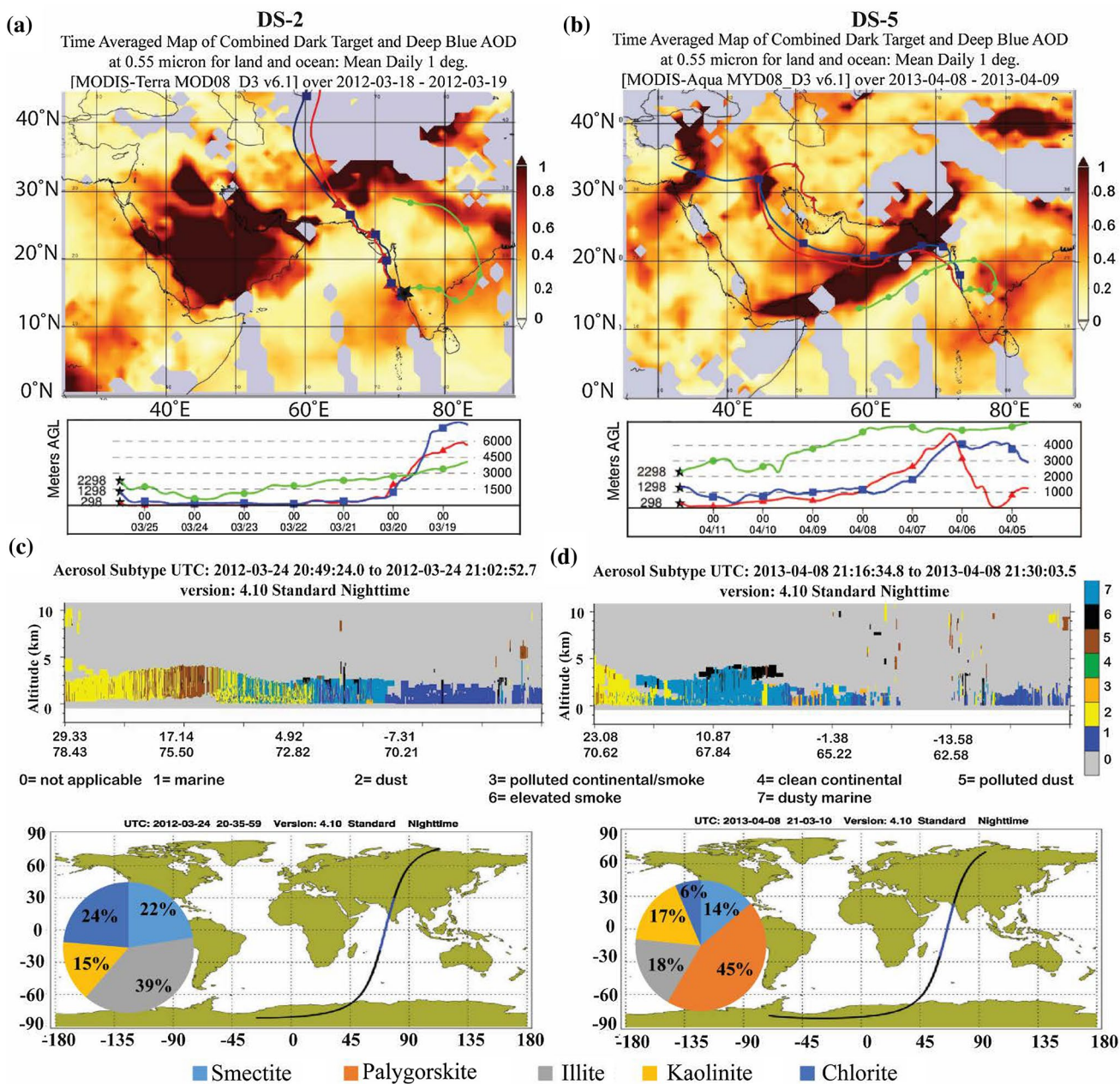


**Fig. 3** Map shows area-averaged AOD superimposed with 7-day air mass back trajectories ending at the Goa on sample collection date for samples collected during dust storm period **a** DS-2 and **b** DS-5. In **a**, the trajectories pass over the high AOD regions of SW Asia. Although high AOD is observed over the Arabian Peninsula, the trajectories show that the dust collected during the DS-2 are mainly

derived from SW Asia. In **b**, trajectories pass over the high AOD regions of the Arabian Peninsula, indicating the dust is from the Arabian sources. CALIPSO passes near the sampling site for the sampling of **c** DS-2 and **d** DS-5, which shows the presence of dust (yellow is dust) over the Arabian Sea region. Also shown the pie chart highlighting relative fraction of clay minerals in dust collected

S2a–S2e). Unlike the wet deposition collection, where winds are constantly from the southwest, large variation in wind patterns is observed during the dry period. As discussed previously, western disturbances are mainly responsible for dust transport; the back trajectories support such transport from the dust emission region which is evident from high AOD values in the SW Asian Desert region as well as in the Arabian Peninsula (Fig. 3a, b). The transport of dust during the dry period is also via high-altitude layers as seen from the CALIPSO profiles shown in Fig. 3c, d. The CALIPSO profile passing through the sampling site (Goa) for DS-2 and DS-5 clearly shows yellow (representing pure dust) and a mix of yellow and brown (representing polluted dust) in respective vertical profiles. These observations highlight the role and importance of high-altitude long-range transport of aeolian dust which can impact remote pristine ocean ecosystem.

### Dust deposition fluxes during the wet and dry period

The wet deposition fluxes show large variation during SW monsoon with values ranging from 63 to 949  $\text{mg m}^{-2} \text{day}^{-1}$  (Table 1) and an average of  $293 \pm 244 \text{ mg m}^{-2} \text{day}^{-1}$ . The wet deposition flux is mainly due to the scavenging of the dust particles in the atmosphere by precipitation. This process is one of the dominant removal processes during the SW monsoon season in this region (the Indian sub-continent). An increasing trend in flux values was observed, from the beginning of the monsoon (in June, the average is  $266 \pm 163 \text{ mg m}^{-2} \text{day}^{-1}$ ) to the middle of monsoon (during July and August average is  $393 \pm 293 \text{ mg m}^{-2} \text{day}^{-1}$ ). Subsequently, it decreases at the end of the monsoon period (in September, the average is  $95 \pm 32 \text{ mg m}^{-2} \text{day}^{-1}$ ) which can be attributed to the reduced rainfall at the end of the monsoon as well as the change in the wind systems that supply dust to the Eastern Arabian Sea such as the Summer Shamal and Red Sea winds (Yu et al. 2016; Rashki et al. 2019).

In the dry season (from October to May), dust storms over the Middle-east and SW Asia are the major contributor of dust which reaches the sampling site (Goa; Aswini et al. 2020; Kumar et al. 2020). In this study, out of the twelve dust storms that impacted the NEAS, five dust storms were during the winter months (October–March) and seven were during the summer season (May to June). The dry deposition fluxes during the dust storm period show a large variation, ranging from 60 to 132  $\text{mg m}^{-2} \text{day}^{-1}$ . The average flux of mineral dust during the winter and summer months is  $102 \text{ mg m}^{-2} \text{day}^{-1}$  and  $91 \text{ mg m}^{-2} \text{day}^{-1}$ , respectively, with total dust dry deposition of  $1147 \text{ mg m}^{-2}$  during the twelve dust storm events to the NEAS. The dust flux during the dry deposition period is mainly due to the gravity settling, and the large variation in this flux may be attributed to dust storm

intensity at the source region and associated wind pattern over the Arabian Sea. During summer months, the majority of dust sources were backtracked to the Arabian Peninsula, and estimated dry deposition flux from this source was averaged at  $108 \pm 8 \text{ mg m}^{-2} \text{day}^{-1}$ . In contrast with this, dust sources backtracked to the SW Asia (during summer and winter) were found to be relatively lower with an average of  $86 \pm 28 \text{ mg m}^{-2} \text{day}^{-1}$ . This indicates the dominant role of the Arabian Peninsula in providing dust to the Arabian Sea during dry months, which have been highlighted by previous studies (Tindale and Pease 1999; Kumar et al. 2008; 2012).

Although the wet deposition flux represents a single-year data, it is evident that the wet deposition fluxes are much higher (more than 4 times) than dry deposition fluxes over the NEAS. To get a global perspective of the daily dust deposition fluxes, we compared our data with the dust fluxes reported at different locations, viz. the coastal stations of UAE (Hamza et al. 2011), which is near the dust source region and a remote location of Kerguelen Island in the Southern Ocean (Heimburger et al. 2013). The average dust flux in the UAE was reported to be  $6380 \text{ g m}^{-2} \text{day}^{-1}$ , in comparison with  $209 \text{ mg m}^{-2} \text{day}^{-1}$  (total dust flux) in the NEAS, whereas the dust flux in the Kerguelen Island is  $0.66 \text{ mg m}^{-2} \text{day}^{-1}$ . The dust flux in the NEAS is very less compared with the UAE (which is one of the major dust source regions), as the dust sources in the region are located far away from the sampling location. Kerguelen Island which is a remote location has very lower dust flux. The settling of the dust and the wind speed during long-range transportation plays a major role in controlling dust flux in the NEAS.

### Clay mineralogical characterization of wet deposited aeolian dust

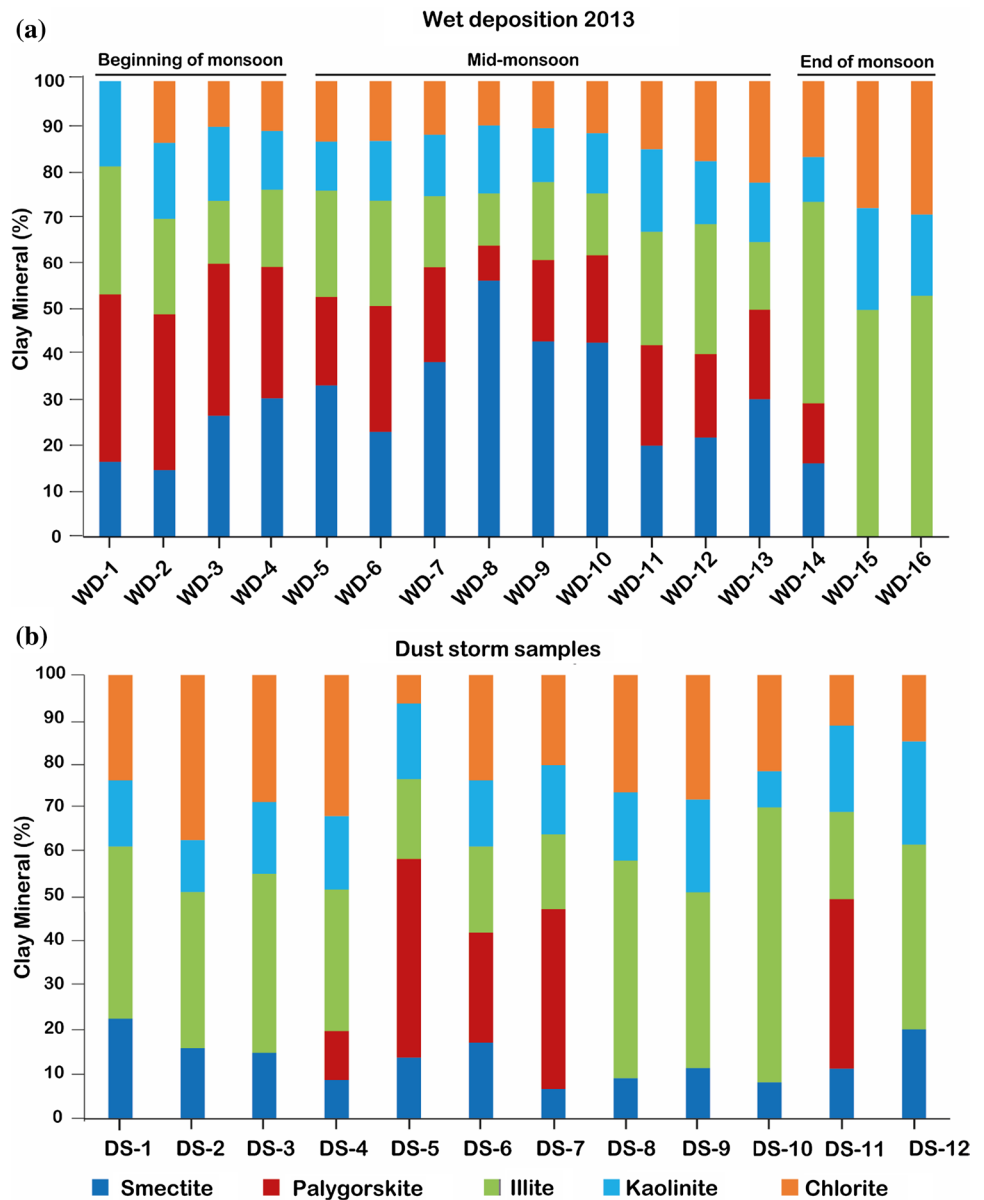
The relative clay mineral percentages for the wet deposition samples collected between June and August (WD-1 and 13) are dominated by smectite (15–56%), followed by illite (11–29%) and palygorskite (8–37%) (Fig. 4a). Palygorskite and smectite were absent in the samples collected during September (except WD-14 which contains 16 and 13% of smectite and palygorskite, respectively), which is dominated by illite (44–53%) and chlorite (28–29%). Kaolinite and chlorite show negligible variations in relative clay mineral abundance throughout the monsoon, except the last two samples collected during September, where kaolinite and chlorite are more than 20%. Illite/kaolinite ratio varied between 0.8 and 2.2 from June to August, and in September, the ratio increases from 2.2 to 4.5. Palygorskite/illite ratio for the samples varied from 0.3 to 2.4.

The presence of illite and palygorskite with an average of 19 and 24 %, respectively, indicates mineral dust contribution from the Arabian Peninsula. Several studies on the Arabian Sea sediments show that the palygorskite is





**Fig. 4** Relative clay mineral percentages of **a** wet deposition dust samples and **b** aerosol samples collected during dust storms



mainly contributed by the dust from the Arabian Peninsula (Debrabant et al. 1991). We find a palygorskite/illite ratio of 0.6–2.4, which is similar to that found in the Arabian Sea sediments off the Yemen-Oman region (Debrabant et al. 1991; Sirocko and Lange 1991). The high smectite content of the wet deposition samples is due to the contribution of dust from the NE African sources, which has abundant smectite in the volcanic regions of African Rift Valley’s Afar triangle and other coastal plains of northeast Africa (Rojas et al. 2019; Sirocko and Lange 1991). The high smectite content of the sample WD-8 is due to the dust emitted from the NE African sources during the preceding days of the sampling, which is evident from the AOD and back trajectories (Fig. S1d of supplementary material S1). In September, the dust is dominated by high illite (44–53 %) and chlorite

(17–29 %) with smectite and palygorskite are absent, thus signifying the change in the dust source region at the end of the SW monsoon period.

High AOD and back trajectories from June to August over this region indicate the transport of dust from NE Africa and the Arabian Peninsula toward NEAS (Fig. 2a). From June to September three major wind systems, (i) the SW monsoon flows toward the Indian sub-continent through the NE Africa (Fig. 1), (ii) summer Shamal winds from the Mediterranean Sea flow through the dust source regions of Tigris-Euphrates floodplains (Syria, Iraq and Kuwait), Ad Dahna and into the Rub Al Khali, picks dust, and flows toward the Arabian Sea (Yu et al. 2016), and (iii) the Red Sea wind blows along with the coastal dust sources of the Red Sea. The dust to the eastern Arabian Sea during the SW monsoon is mainly

carried at 2–5 km altitude, by the dusty continental winds like Summer Shamal and the Red Sea winds riding above the humid SW monsoon winds (Ramaswamy et al. 2017; Suresh et al. 2021).

### Clay mineralogical characterization of dry deposited aeolian dust

Out of the 12 dust sample collection (DS-1, DS-2, DS-3, DS-8, DS-9, and DS-12), six have relatively abundant illite (35–49 %), chlorite (15–37 %), with moderate kaolinite (12–23 %), smectite (9–23 %), and no traces of palygorskite (Fig. 4b). Illite-to-kaolinite ratios for these samples collected during dust storm range from 1.8 to 3.2. DS-10 contains illite close to 62 % and chlorite 22%. Smectite and kaolinite make 8% each, and palygorskite is absent. Illite/kaolinite ratio for this dust storm sample is 7.5. Five dust samples (DS-4, DS-5, DS-6, DS-7, and DS-11) contain palygorskite (11–45 %) with moderate illite (17–32 %) and chlorite (6–32 %). Illite/kaolinite and palygorskite/illite ratio for these samples range from 1 to 1.9 and 1.3 to 2.5 (excluding DS-4), respectively. In the dry season (from October to May), the dust storm events are the major contributor of dust, as many dust plumes that originate from the Middle-east and SW Asia reach the NEAS (Kumar et al. 2020). Out of the twelve dust storms that reached the NEAS, five dust storms were during the winter months (October–March) and seven were during the summer months (May to June).

Unlike the wet deposition samples collected during the SW monsoon period, the clay mineralogy of the twelve dry deposition samples is significantly different and varied with each dust storm. Dust samples sourced from SW Asia (DS-1, DS-2, DS-3, DS-8, DS-9, and DS-12) have high illite (35–49 %), chlorite (15–37 %), low kaolinite (12–23 %), and smectite (9–23 %), with the absence of palygorskite. Illite-to-kaolinite ratios of 1.8–3.2 are similar to the sediments off the Makran coast, indicating similar clay mineralogy of SW Asian source (Sirocko and Lange 1991). Back trajectories and AOD for preceding days of sample collection indicate that sources of dust emissions were from any of the source areas like the Sistan basin, Jaz Murian basin, Makran coast, and other endorheic basins of SW Asia. Dust sample (DS-10) is mainly derived from the Indus Delta flood plains which is evident from very high illite (62 %) and chlorite content. Illite/kaolinite ratio for this dust storm sample is 7.5, which is similar to those reported for the Indus sediments (Alizai et al. 2012). Dust samples (DS-5, 6, 7, and 11), which were found to be originated from the Arabian Peninsula, have a higher abundance of palygorskite (25–45%) with moderate illite (17–20%) and chlorite (6–24 %). Palygorskite-to-illite ratio was found to be in the range of 1.3–2.5, which is similar to those reported for the sediments off the Arabian Peninsula (Sirocko and Lange 1991). Dust sample

DS-4 shows a mixed signature of the Arabian Peninsula and SW Asian sources. This sample contains minor palygorskite (11%), moderate illite (32 %), chlorite (32 %), and very low smectite with an illite/kaolinite ratio of 1.9. A careful study of the AOD map (Fig S2b in Supplementary material S1) indicates two dust outbreaks on February 4, 2013, in the coastal Oman region (Arabian Peninsula) as well as the Helmand basin in the SW Asian Desert region. 7-day back trajectories reaching the sampling site were found to traverse through these regions (Fig. S2b), possibly picking up dust from both outbreaks; thus, a mixed signature of both sources was observed. Based on satellite images and clay composition, seven were found to derive from SW Asian sources, four were from the Arabian Peninsula, and one was found to be a mixture of both regions.

### Seasonal variation in dust characteristics over the NEAS

Seasonal variations in the dust to the northeastern Arabian Sea are due to the change in the wind systems responsible for the transportation of mineral dust from the sources. The wind systems during the SW monsoon (June–September) are consistent and blow with high speeds over the same dust sources for an extended period. Hence, the clay mineralogy of wet deposition samples of June to August does not show any significant variations, and the wet deposition flux during this period is also high. At the end of the SW monsoon (September), there is a significant change from high to low deposition flux. Also, the clay mineral composition changes from palygorskite and smectite dominated (June to August) to illite and chlorite dominated samples indicating the significant impact of SW Asian source (Fig. 4a note end of monsoon samples). By this time, the summer Shamal winds have seized (Yu et al. 2016), and the ITCZ starts migrating south; dust activity in the endorheic basins of SW Asia continues till September due to the persistent Levant winds (Alizadeh-Choobari et al. 2014; Rashki et al. 2019). The back trajectories show the flow of air mass from SW Asia toward the eastern Arabian Sea (Fig. 2b) for the samples collected during September, suggesting the change in the source which is responsible for the change in the mineralogical characteristics of dust at the end of the monsoon. On the other hand, the dust storm samples collected during the dry period are episodic and no significant temporal variability in characteristic mineralogical composition was observed. The clay mineralogy of these dust samples varies considerably depending on the passage of the winter Shamal over different source regions, favorable wind pattern as well as dust emission intensity in the source region.

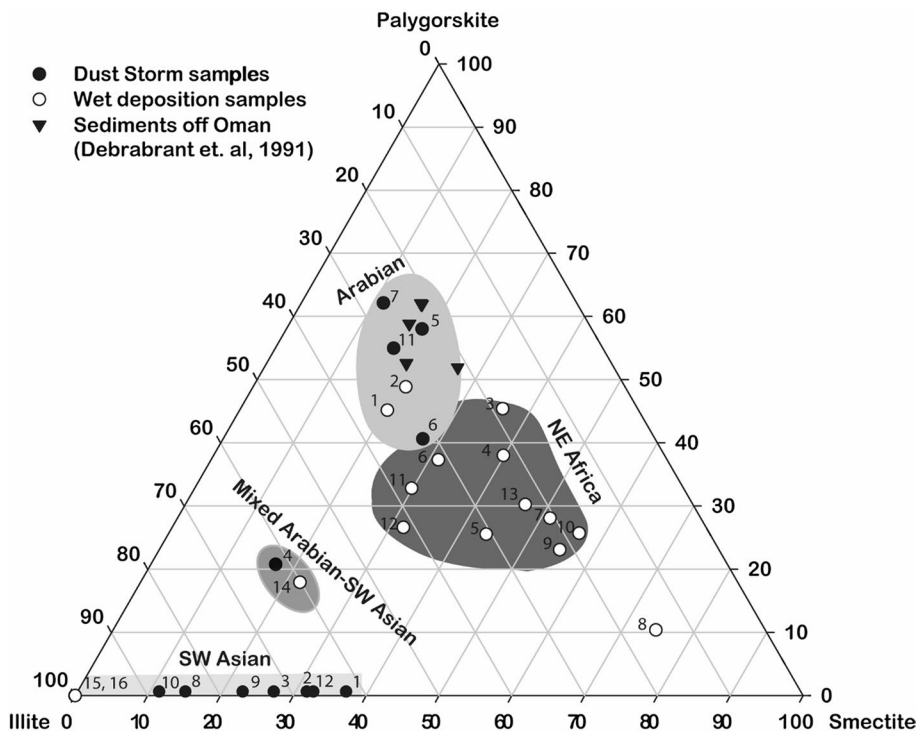
Both wet and dry deposition samples of Arabian Peninsula origin show the presence of palygorskite; however, wet deposition samples collected from June to August have

moderate to abundant smectite. In contrast, the dust samples collected during the dry period show distinctly lower smectite compared to wet deposition samples collected from June to August. This difference in the smectite percentage is due to the dust contribution from the active sources of north-eastern Africa during the SW monsoon (Ramaswamy et al. 2017). We used a ternary plot (composed of palygorskite, illite, and smectite) to further assess the relative contribution from different sources (Fig. 5). Overall, 3 different clusters were observed: (1) High palygorskite with moderate smectite and minor illite content which highlight the dominant Arabian Peninsula source; (2) High smectite with moderate palygorskite and minor illite content representing dominant NE African source; (3) High illite with negligible palygorskite and smectite content representing dominant SW Asian sources. In this diagram, most of the wet deposited samples (WDS) were found to fall in the 2nd cluster which has relatively high smectite with moderate palygorskite content and indicates the dominance of the NE African source contribution. However, few samples were observed in the 1st cluster having higher palygorskite content indicating the significant contribution from the Arabian Peninsula end member. Interestingly, there was no significant contribution observed from SW Asia as insignificant illite content was found for the majority of WDS samples except WD-14, 15, and 16 which were collected at the end of the monsoon period (in September). This inference from the ternary diagram corroborates with those preliminary observations from the AOD maps, 7-day back trajectory analyses, as well as CALIPSO

that passes during the SW monsoon months. In the case of samples collected during dry months, the majority of them were falling in the clusters defined by the Arabian Peninsula and SW Asian sources. It is important to highlight here that most of the dust samples (in dry period) were collected during the summer season (March–June) and around 50 % (DS-5, 6, 7, 11) of them were found to fall in the Arabian Peninsula cluster with relatively higher palygorskite content (Fig. 5). One sample DS-4, which was collected in the winter month, has relatively lower palygorskite and high illite content suggesting a mixed contribution from the SWA and Arabian Peninsula sources. However, the rest of the samples collected in the winter months (DS-3 and DS-10) as well as in summer (DS-1, 2, 8, 9, 12) have a dominant contribution from the SW Asian sources evident from the high illite content with negligible palygorskite and smectite content. This interpretation of significant contribution from the SWA and Arabian sources during the dry period is also supported by satellite images/data and back trajectory analyses discussed in previous sections.

Based on this ternary plot as well as the remote sensing data, overall significant sources contributing to dust over the Arabian Sea and their season variability in the mineralogical composition are as follows: (1) Arabian Peninsula contributing during the wet and dry period; (2) the NE Africa which is significant during the SW monsoon months only; and (3) The SW Asian sources which contribute during summer and winter month during the dry period as well as at the end of monsoon. These results corroborate with those discussed in

**Fig. 5** Ternary diagram showing clay mineral composition indicating the Arabian, mixed Arabian–NE African, SW Asian, and mixed Arabian–SW Asian sources



previous publication wherein radiogenic isotopic (Sr–Nd) composition has been used to identify sources of Aeolian dust over the Arabian Sea (Kumar et al. 2020; Suresh et al. 2021). It is important to mention that the temporal variability during the SW monsoon months as well as source attribution in the dry and wet periods, reported here, is based on one-year data (during the SW monsoon) as well as few dust events (during the dry period). The robustness of this temporal variability and dust source contribution to the Arabian Sea can be further ascertained by analyzing long-term (4–5 years) geochemical proxies of mineral dust at coastal locations over the NEAS.

## Conclusion and implications

This study reports quantification of dust fluxes during wet and dry period over the NEAS, their clay mineralogical composition, and its seasonal variation. The following are the major outcome from this study:

1. Wet deposition fluxes were found to be significantly higher than dry deposition fluxes estimated during the dust storm period at this study site.
2. Large variability in deposition fluxes was observed for the dry and wet periods and had been attributed to the favorable meteorological condition as well as dust emission intensity at the source region.
3. The wet deposition fluxes were found to show an increasing trend from the beginning of monsoon (June) till mid of monsoon (July–August) and subsequently found to decline at the end of the monsoon (in September).
4. There was no significant temporal variability observed for the dry period; however, higher fluxes were found for those samples collected in dust storm events over the Arabian Peninsula as compared to those derived from the SW Asian desert region.
5. AOD maps, 7-day back trajectories, as well as CALIPSO images, were used for preliminary identification of dust emission source regions as well as their transport to the sampling site via the Arabian Sea during the wet and dry period.
6. The clay mineral composition displays significant differences for wet and dry deposited aeolian dust. Those deposited during SW monsoon have high palygorskite and smectite, with moderate illite content; however, dry deposited dust is mainly characterized by high illite and chlorite content. Palygorskite was also found in some of the dry deposited samples. These seasonal variations in mineral content point to change in dust emission sources over the Arabian Sea.
7. Using clay mineral composition and their ratio, an attempt has been made to identify sources of mineral

dust. Arabian Peninsula and northeast Africa were found to contribute significantly during the SW monsoon (wet period); however, southwest Asia and Arabian Peninsula were major sources during the dry season. These source identifications were corroborated with satellite retrieval and back trajectory analyses.

The clay mineral composition reported in this study has been used as a robust proxy to understand paleo-monsoon as well as modern and paleo-dust circulation. This study will provide very significant information on the composition of clay minerals in the aeolian dust, which will further help in assessing relative contribution from fluvial vis-à-vis aeolian fluxes to the Arabian Sea. In addition, the clay composition of dust is critical in assessing the radiative impact due to mineral dust, as varying clay minerals have a different refractive index. Thus, the reported dataset on clay minerals can be used in Earth's radiative budget models as well as biogeochemical models for the projection of processes linked with future climate change.

**Supplementary Information** The online version contains supplementary material available at <https://doi.org/10.1007/s13762-021-03503-y>.

**Acknowledgements** We gratefully acknowledge the NOAA Air Resources Laboratory (ARL) for the provision of the HYSPLIT transport and dispersion model (<http://www.ready.noaa.gov>) used in this publication. Discussion with Dr. Namandeep Singh and his comments was helpful and constructive. We thank the two anonymous reviewers and editor for their valuable comments/suggestions, which helped in improving this paper. NIO Contribution number is 6761.

**Funding** Funding for this research is partially supported by CSIR Networked Project GEOSINK. Ashwini Kumar and K Suresh were funded by the Department of Science and Technology, Govt. of India, under the INSPIRE Faculty scheme (IFA13-EAS-13), SPLICE Program (Grant No. DST/CCP/Aerosol/85/2017(G)) and INSPIRE Research Fellowship (IF140405), respectively.

## Compliance with ethical standards

**Ethical approval** This article does not contain any studies with human participants or animals performed by any of the authors.

## References

- Alaily F (1995) Soil properties of quaternary deposits in the arid part of northeastern Somalia. *Arid Land Res Manag* 9(1):39–50
- Alizadeh-Choobari O, Zawar-Reza P, Sturman A (2014) The “wind of 120 days” and dust storm activity over the Sistan Basin. *Atmos Res* 143:328–341. <https://doi.org/10.1016/j.atmosres.2014.02.001>
- Alizai A, Hillier S, Clift PD, Giosan L, Hurst A, VanLaningham S, Macklin M (2012) Clay mineral variations in Holocene terrestrial sediments from the Indus Basin. *Quat Res* 77:368–381. <https://doi.org/10.1016/j.yqres.2012.01.008>
- Anderson RF, Cheng H, Edwards RL, Fleisher MQ, Hayes CT, Huang KF et al (2016) How well can we quantify dust



- deposition to the ocean? *Philos Trans R Soc A Math Phys Eng Sci* 374(2081):20150285
- Aswini MA, Kumar A, Das SK (2020) Quantification of long-range transported aeolian dust towards the Indian peninsular region using satellite and ground-based data—a case study during a dust storm over the Arabian Sea. *Atmos Res* 239:104910. <https://doi.org/10.1016/j.atmosres.2020.104910>
- Avinash K, Kurian PJ, Warriar AK, Shankar R, Vineesh TC, Ravindra R (2016) Sedimentary sources and processes in the eastern Arabian Sea: insights from environmental magnetism, geochemistry and clay mineralogy. *Geosci Front* 7(2):253–264
- Badarinath KVS, Kharol SK, Sharma AR, Ramaswamy V, Kaskaoutis DG, Kambezidis HD (2009) Investigations of an intense aerosol loading during 2007 cyclone SIDR: a study using satellite data and ground measurements over Indian region. *Atmos Environ* 43:3708–3716. <https://doi.org/10.1016/j.atmosenv.2009.04.026>
- Badarinath KVS, Kharol SK, Kaskaoutis DG, Sharma AR, Ramaswamy V, Kambezidis HD (2010) Long-range transport of dust aerosols over the Arabian Sea and Indian region: a case study using satellite data and ground-based measurements. *Glob Planet Change* 72:164–181. <https://doi.org/10.1016/j.gloplacha.2010.02.003>
- Banerjee P, Prasanna Kumar S (2014) Dust-induced episodic phytoplankton blooms in the Arabian Sea during winter monsoon. *J Geophys Res C Ocean* 119:7123–7138. <https://doi.org/10.1002/2014JC010304>
- Biscaye PE (1965) Mineralogy and sedimentation of recent deep-sea clay in the Atlantic Ocean and adjacent seas and oceans. *Geol Soc Am Bull* 76(7):803–832
- Caquineau S, Gaudichet A, Gomes L, Legrand M (2002) Mineralogy of Saharan dust transported over northwestern tropical Atlantic Ocean in relation to source regions. *J Geophys Res Atmos*. <https://doi.org/10.1029/2000JD000247>
- Claquin T, Schulz M, Balkanski YJ (1999) Modeling the mineralogy of atmospheric dust sources. *J Geophys Res Atmos* 104:22243–22256
- Claquin T, Roelandt C, Kohfeld KE, Harrison SP, Tegen IC, Balkanski PI, Bergametti Y, Hansson G, Mahowald M, Rodhe NM, Schulz HM (2003) Radiative forcing of climate by ice-age atmospheric dust. *Clim Dyn* 20:193–202. <https://doi.org/10.1007/s00382-002-0269-1>
- Coale KH, Johnson KS, Fitzwater SE, Gordon RM, Tanner S, Chavez FP et al (1996) A massive phytoplankton bloom induced by an ecosystem-scale iron fertilization experiment in the equatorial Pacific Ocean. *Nature* 383(6600):495–501
- Debrabant P, Krissek L, Bouquillon A, Chamley H (1991) Clay mineralogy of neogene sediments of the Western Arabian Sea: mineral abundances and paleoenvironmental implications. *Proc Ocean Drill Prog Sci Results* 117:183–196. <https://doi.org/10.2973/odp.proc.sr.117.137.1991>
- Duce RA, Tindale NW (1991) Atmospheric transport of iron and its deposition in the ocean. *Limnol Oceanogr* 36(8):1715–1726
- Duce RA, Liss PS, Merrill JT, Atlas EL, Buat-Menard P, Hicks BB et al (1991) The atmospheric input of trace species to the world ocean. *Glob Biogeochem Cycles* 5(3):193–259
- Ginoux P, Chin M, Tegen I, Prospero JM, Holben B, Dubovik O, Lin S-J (2001) Sources and distributions of dust aerosols simulated with the GOCART model. *J Geophys Res Atmos* 106:20255–20273. <https://doi.org/10.1029/2000JD000053>
- Goudie AS, Middleton NJ (2006) *Desert dust in the global system*. Springer, New York
- Guiou C, Al Azhar M, Aumont O, Mahowald N, Levy M, Ethé C, Lachkar Z (2019) Major impact of dust deposition on the productivity of the Arabian Sea. *Geophys Res Lett*. <https://doi.org/10.1029/2019GL082770>
- Hamza W, Enan MR, Al-Hassini H, Stuu JB, De-Beer D (2011) Dust storms over the Arabian Gulf: a possible indicator of climate changes consequences. *Aquat Ecosyst Health Manag* 14(3):260–268
- Heimburger A, Losno R, Triquet S (2013) Solubility of iron and other trace elements in rainwater collected on the Kerguelen Islands (South Indian Ocean). *Biogeosciences* 10(10):6617–6628
- Jickells T, Moore CM (2015) The importance of atmospheric deposition for ocean productivity. *Annu Rev Ecol Evol S* 46:481–501
- Jickells TD, An ZS, Andersen KK, Baker AR, Bergametti G, Brooks N et al (2005) Global iron connections between desert dust, ocean biogeochemistry, and climate. *Science* 308(5718):67–71
- Jickells T, Baker A, Chance R (2016) Atmospheric transport of trace elements and nutrients to the oceans. *Philos Trans R Soc A* 374:20150286. <https://doi.org/10.1098/rsta.2015.0286>
- Kiefert L, McTainsh GH, Nickling WG (1992) Pretreatment techniques for particle-size analysis of dust samples from high volume sampler filter papers. *J Sedim Res* 62(4):729–731
- Kok JF, Adebisi AA, Albani S, Balkanski Y, Checa-Garcia R, Chin M et al (2021) Contribution of the world's main dust source regions to the global cycle of desert dust. *Atmos Chem Phys Discuss*. <https://doi.org/10.5194/acp-2021-4>
- Kumar A, Sarin MM (2009) Mineral aerosols from western India: temporal variability of coarse and fine atmospheric dust and elemental characteristics. *Atmos Environ* 43(26):4005–4013
- Kumar A, Sarin MM, Sudheer AK (2008) Mineral and anthropogenic aerosols in Arabian Sea—atmospheric boundary layer: sources and spatial variability. *Atmos Environ* 42(21):5169–5181
- Kumar A, Sudheer AK, Goswami V, Bhusan R (2012) Influence of continental outflow on aerosol chemical characteristics over the Arabian Sea during winter. *Atmos Environ* 50:182–191
- Kumar A, Suresh K, Rahaman W (2020) Geochemical characterization of modern aeolian dust over the Northeastern Arabian Sea: implication for dust transport in the Arabian Sea. *Sci Total Environ* 729:138576. <https://doi.org/10.1016/j.scitotenv.2020.138576>
- Léon J, Legrand M (2003) Mineral dust sources in the surroundings of the north Indian Ocean. *Geophys Res Lett*. <https://doi.org/10.1029/2002GL016690>
- Madhura RK, Krishnan R, Revadekar JV, Mujumdar M, Goswami BN (2014) Changes in western disturbances over the Western Himalayas in a warming environment. *Clim Dyn* 44:1157–1168. <https://doi.org/10.1007/s00382-014-2166-9>
- Mahowald NM, Baker AR, Bergametti G, Brooks N, Duce RA, Jickells TD, Kubilay N, Prospero JM, Tegen I (2005) Atmospheric global dust cycle and iron inputs to the ocean. *Glob Biogeochem Cycles*. <https://doi.org/10.1029/2004GB002402>
- Mahowald NM, Hamilton DS, Mackey KR, Moore JK, Baker AR, Scanza RA, Zhang Y (2018) Aerosol trace metal leaching and impacts on marine microorganisms. *Nat Commun* 9:2614. <https://doi.org/10.1038/s41467-018-04970-7>
- McLennan SM (2001) Relationships between the trace element composition of sedimentary rocks and upper continental crust. *Geochem Geophys Geosyst* 2:4
- Moore JK, Lindsay K, Doney SC, Long MC, Misumi K (2013) Marine ecosystem dynamics and biogeochemical cycling in the Community Earth System Model [CESM1 (BGC)]: comparison of the 1990s with the 2090s under the RCP4.5 and RCP8.5 scenarios. *J Clim* 26(23):9291–9312
- Okin GS, Mahowald N, Chadwick OA, Artaxo P (2004) Impact of desert dust on the biogeochemistry of phosphorus in terrestrial ecosystems. *Glob Biogeochem Cycles*. <https://doi.org/10.1029/2003GB002145>
- Paytan A, Mackey KR, Chen Y, Lima ID, Doney SC, Mahowald N et al (2009) Toxicity of atmospheric aerosols on marine phytoplankton. *Proc Natl Acad Sci* 106(12):4601–4605



- Pease PP, Tchakerian VP, Tindale NW (1998) Aerosols over the Arabian Sea: geochemistry and source areas for aeolian desert dust. *J Arid Environ* 39(3):477–496
- Prospero JM, Ginoux P, Torres O, Nicholson SE, Gill TE (2002) Environmental characterization of global sources of atmospheric soil dust identified with the NIMBUS 7 Total Ozone Mapping Spectrometer (TOMS) absorbing aerosol product. *Rev Geophys* 40:1–31. <https://doi.org/10.1029/2000RG000095>
- Purnachandra Rao V, Shynu R, Singh SK, Naqvi SWA, Kessarkar PM (2015) Mineralogy and Sr-Nd isotopes of SPM and sediment from the Mandovi and Zuari estuaries: influence of weathering and anthropogenic contribution. *Estuar Coast Shelf Sci* 156:103–115. <https://doi.org/10.1016/j.ecss.2014.07.004>
- Ramaswamy V (2014) Influence of tropical storms in the northern Indian Ocean on dust entrainment and long-range transport. In: *Typhoon impact and crisis management*. Springer, Berlin, Heidelberg, pp 149–174
- Ramaswamy V, Muraleedharan PM, Babu CP (2017) Mid-troposphere transport of Middle-East dust over the Arabian Sea and its effect on rainwater composition and sensitive ecosystems over India. *Sci Rep* 7:1–8. <https://doi.org/10.1038/s41598-017-13652-1>
- Rashki MNJ, Goudie AS (2021) Dust storms in Iran: distribution, causes, frequencies and impacts. *Aeolian Res* 48:100655. <https://doi.org/10.1016/j.aeolia.2020.100655>
- Rashki A, Kaskaoutis DG, Sepehr A (2018) Statistical evaluation of the dust events at selected stations in Southwest Asia: from the Caspian Sea to the Arabian Sea. *CATENA* 165:590–603
- Rashki A, Kaskaoutis DG, Mofidi A, Minvielle F, Chiapello I, Legrand M, Francois P (2019) Effects of monsoon, Shamal and Levar winds on dust accumulation over the Arabian Sea during summer—The July 2016 case. *Aeolian Res* 36:27–44
- Rojas VP, Meynadier L, Colin C, Bassinot F, Valet JP, Miska S (2019) Multi-tracer study of continental erosion and sediment transport to the Red Sea and the Gulf of Aden during the last 20 ka. *Quat Sci Rev* 212:135–148. <https://doi.org/10.1016/j.quascirev.2019.02.033>
- Rolph G, Stein A, Stunder B (2017) Real-time environmental applications and display system: READY. *Environ Model Softw* 95:210–228
- Shelley RU, Morton PL, Landing WM (2015) Elemental ratios and enrichment factors in aerosols from the US-GEOTRACES North Atlantic transects. *Deep Sea Res II Top Stud Oceanogr* 116:262–272
- Singer A, Stahr K, Zarei M (1998) Characteristics and origin of sepiolite (Meerschaum) from Central Somalia. *Clay Miner* 33:349–362. <https://doi.org/10.1180/000985598545525>
- Sirocko F, Lange H (1991) Clay-mineral accumulation rates in the Arabian Sea during the late Quaternary. *Mar Geol* 97:105–119. [https://doi.org/10.1016/0025-3227\(91\)90021-U](https://doi.org/10.1016/0025-3227(91)90021-U)
- Stein AF, Draxler RR, Rolph GD, Stunder BJB, Cohen MD, Ngan F (2015) NOAA's HYSPLIT atmospheric transport and dispersion modeling system. *Bull Am Meteorol Soc* 96:2059–2077. <https://doi.org/10.1175/BAMS-D-14-00110.1>
- Suresh K, Singh U, Kumar A, Karri D, Peketi A, Ramaswamy V (2021) Provenance tracing of long-range transported dust over the North-eastern Arabian Sea during the southwest monsoon. *Atmos Res* 250:105377
- Swap R, Garstang M, Greco S, Talbot R, Kållberg P (1992) Saharan dust in the Amazon Basin. *Tellus*. <https://doi.org/10.1034/j.1600-0889.1992.t01-1-00005.x>
- Tegen I, Lacis AA, Fung I (1996) The influence on climate forcing of mineral aerosols from disturbed soils. *Nature* 380:419–422. <https://doi.org/10.1038/380419a0>
- Thoppil PG, Hogan PJ (2010) Persian Gulf response to a wintertime shamal wind event. *Deep Res I Oceanogr Res Pap* 57:946–955. <https://doi.org/10.1016/j.dsr.2010.03.002>
- Tindale NW, Pease PP (1999) Aerosols over the Arabian Sea: atmospheric transport pathways and concentrations of dust and sea salt. *Deep Sea Res II Top Stud Oceanogr* 46(8–9):1577–1595
- Vaughan MA, Young SA, Winker DM, Powell KA, Omar AH, Liu Z ... Hostetler CA (2004, November) Fully automated analysis of space-based lidar data: an overview of the CALIPSO retrieval algorithms and data products. In *Laser radar techniques for atmospheric sensing*, vol 5575. International Society for Optics and Photonics, pp 16–30
- Vinoy V, Rasch PJ, Wang H, Yoon J, Ma P, Landu K, Singh B (2014) Short-term modulation of Indian summer monsoon rainfall by West Asian dust. *Nat Geosci* 7:308–313. <https://doi.org/10.1038/NNGEO2107>
- Vögeli N, van der Beek P, Huyghe P, Najman Y (2017) Weathering in the Himalaya, an East-West comparison: indications from major elements and clay mineralogy. *J Geol* 125(5):515–529
- Watson AJ, Bakker DCE, Ridgwell AJ, Boyd PW, Law CS (2000) Effect of iron supply on Southern Ocean CO<sub>2</sub> uptake and implications for glacial atmospheric CO<sub>2</sub>. *Nature* 407(6805):730–733
- Winker DM, Vaughan MA, Omar A, Hu Y, Powell KA, Liu Z et al (2009) Overview of the CALIPSO mission and CALIOP data processing algorithms. *J Atmos Oceanic Technol* 26(11):2310–2323
- Yu Y, Notaro M, Kalashnikova OV, Garay MJ (2016) Climatology of summer Shamal wind in the Middle East. *J Geophys Res Atmos* 121:289–305. <https://doi.org/10.1002/2015JD024063>
- Yu Z, Colin C, Wan S, Saraswat R, Song L, Xu Z, Clift P, Lu H, Lyle M, Kulhanek D, Hahn A, Tiwari M, Mishra R, Miska S, Kumar A (2019) Sea level-controlled sediment transport to the eastern Arabian Sea over the past 600 kyr: clay minerals and Sr-Nd isotopic evidence from IODP site U1457. *Quat Sci Rev* 205:22–34. <https://doi.org/10.1016/j.quascirev.2018.12.006>

